Transverse thermoelectric effects in platinum strips on permalloy films

S. H. Wang, L. K. Zou, J. W. Cai, B. G. Shen, and J. R. Sun*

Beijing National Laboratory for Condensed Matter Physics and Institute of Physics, Chinese Academy of Sciences, Beijing 100190, People's Republic of China

(Received 20 July 2013; revised manuscript received 1 November 2013; published 20 December 2013)

A comprehensive study on thermoelectric effects is performed for the transverse Pt strips attached to a longitudinal permalloy (Py) layer or sandwiched between two longitudinal Py layers. Thermal voltages jointly determined by planar Nernst effect (PNE), anomalous Nernst effect (ANE), and spin Seebeck effect (SSE) are detected across the Pt strip when a thermal gradient exists. By comparing the data of two differently structured samples, the respective contributions of the PNE, ANE, and SSE to thermal voltage are determined, and they have the ratio of 64:26:10, without considering the shunting effect of conductive Py, or 35:15:50, after the shunting-effect correction.

DOI: 10.1103/PhysRevB.88.214304 PACS number(s): 72.15.Jf, 72.20.Pa, 85.80.−b

I. INTRODUCTION

Generation and detection of spin current are key technologies for spintronics.[1] Spin Hall effect[2,3] and spin pumping effect[4] are viable ways of producing spin current. In addition to these two effects, the spin Seebeck effect (SSE) of the ferromagnet/nonmagnet hybrid structures, a thermoelectric effect arising from the spin injection driven by temperature gradient,[5] provides an alternative approach towards spin manipulation. As theoretically demonstrated, electrons with opposite spin states will have different chemical potentials when a magnet is subjected to a temperature gradient, and this in turn produces a spin current that can be sensed, via inverse spin Hall effect (ISHE), by a nonmagnet strip attached to the magnet.[5] The SSE seems to be a general feature of magnetic materials, and has been observed in various materials, such as ferromagnetic metals,[5] half-metal,[6] semiconductors,[7] insulators,[8,9] and even nonmagnetic semiconductors.[10]

However, whether the detected signals stem from the SSE or not is still under strong debate. Huang *et al.*[11] believed that, for the widely studied permalloy-platinum (Py-Pt) structure, coexisting longitudinal and perpendicular temperature gradients will cause an anomalous Nernst effect (ANE) that admixes with the SSE. They further demonstrated that the Pt layer above $Y_3Fe_5O_{12}$ (YIG) with only a perpendicular thermal gradient could be polarized by magnetic proximity effect, also showing an ANE.[12] To avoid the magnetizing effect of Pt, Qu *et al.*[13] replaced Pt with Au in the above device, and detected a SSE voltage. Since the SSE signal is nearly two orders of magnitude lower than that of Pt, the authors believed that the intrinsic SSE is rather weak. This conclusion seems to be supported by a subsequent investigation of another group. In a deliberately designed Py-Pt structure that completely excludes the ANE, Avery *et al.*[14] observed only a planar Nernst effect (PNE), without any signatures of SSE. On the contrary, Kikkawa *et al.*[15] argued that it was SSE rather than the ANE of polarized Pt that dominated the thermoelectric effect since a sizable thermal voltage survived after sandwiching a 13-nm-thick Cu layer between Pt and YIG. Also, Meier *et al.*[16] declared that for the Pt/$NiFe_2O_4$ hybrid structure the SSE is dominative, and the ANE accounted for only one fourth of the detected thermal voltage. Obviously, the works about SSE conflict strongly with each other, and further studies are required to clarify these points of confusion. For this purpose, we performed a comprehensive study on the thermoelectric effects of the Pt/Py system by deliberately designing sample structure to focus on distinctive thermal effects. It was found that the thermal voltage across the transverse Pt strip was jointly determined by the PNE, ANE, and SSE in the coexistence of longitudinal and perpendicular thermal gradients, and the relative contributions of these three effects, for the typical sample with a Pt layer of 5 nm in thickness, are about 64:26:10, without considering the shunting effect of conductive Py, or 35:15:50, after the shunting-effect correction for the present experiment setup.

II. EXPERIMENTAL PROCEDURES

In total, five samples were prepared for the present experiments following the procedures below. A Py ($Ni_{81}Fe_{19}$) layer with the plane dimension of $10 \times 3\ mm^2$ and the thickness of 25 nm was first deposited by magnetron sputtering on a thermally oxidized Si substrate (0.5 mm in thickness). After an interruption of 5 min, a second Py layer, also 25 nm in thickness, was prepared exactly above the first one, where the intermediate interruption was introduced to mimic the preparation condition of the samples with sandwiched Pt strips as will be described later. To define an easy magnetic axis (EMA) for the Py layer, a magnetic field of about 300 Oe was applied along the long dimension (x axis) of the film during the deposition. Afterwards, two transverse Pt strips with the width of 0.1 mm, the thickness of 5 nm, and the separation of 6 mm were sputtered on the Py layer as SSE detectors. The sample thus obtained will be denoted as sample 1 hereafter. The second sample (sample 2), which was designed in an attempt to eliminate the SSE, was prepared following exactly the same procedures described above except that the two Pt strips were sandwiched between the first and second Py layers. For comparison, other two samples (samples 3 and 4) have exactly the same structure as samples 1 and 2, respectively, except thinner Pt bars (2 nm), were prepared. To clarify the effect of EMA, a fifth sample that has the same configuration as sample 1 but has an EMA along the short axis (y axis) of the Py layer was also prepared (sample 5). For clarity, in Table I we tabulated all the samples studied.

TABLE I. Sample structures.

Sample no.	Structure	EMA (axis)
1	Py(25 nm)/Py(25 nm)/Pt(5 nm)	x
2	Py(25 nm)/Pt(5 nm)/Py(25 nm)	x
3	Py(25 nm)/Py(25nm)/Pt(2 nm)	x
4	Py(25 nm)/Pt(2 nm)/Py(25 nm)	x
5	Py(25 nm)/Py(25 nm)/Pt(5 nm)	y

A 100-Ω heater was placed under a copper block underneath one end of the substrate, and the opposite end of the substrate was kept at ambient temperature by another copper block. The distance between the two blocks is 8 mm. The sample was so positioned that the two Pt strips were located at exactly the middle of the two blocks. Thermal grease was used to get a good thermal contact. The experimental installation was sealed in a metallic box to depress electromagnetic noise and the temperature fluctuation caused by airflow. A step-heating procedure was adopted to establish a temperature gradient, and the temperature difference of the hot and cold ends is set to 30 K. Silver paste was used to connect lead lines (Cu wires) to platinum strips. A nanovoltmeter (Keithley 2182A) was used to measure the transverse voltage across the Pt strips. The measurement was performed after stabilizing the sample for 1 h. A magnetic field was applied in the film plane at an angle with the direction of the longitudinal thermal gradient. A sketch diagram for the experiment setup is shown in Fig. 1.

III. RESULTS AND DISCUSSIONS

To verify magnetic anisotropy, magnetizations (M) along the long and short axes of the samples were measured. As an example, in Fig. 2 we show the experiment results for sample 1. An idealized rectangle-shaped M-H loop is obtained for the magnetic cycling along the x axis, whereas a tilted elliptic M-H loop is detected along the y axis. The coercive force is ~2 Oe, a typical value of the Py films. The difference of the magnetic loops along two orthogonal directions confirms an EMA along the x axis. As designed, all the samples except sample 5, which exhibits an EMA along the y axis, have the same EMA along the x axis.

As reported, either PNE or ANE and SSE (if it exists) can contribute to thermal voltage whenever the thermal gradient

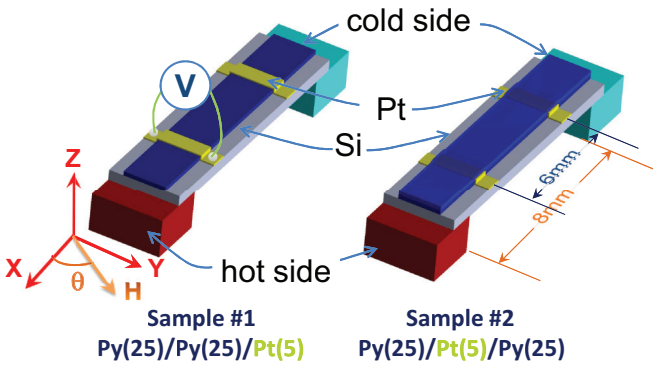

FIG. 1. (Color online) A sketch diagram for experiment setup.

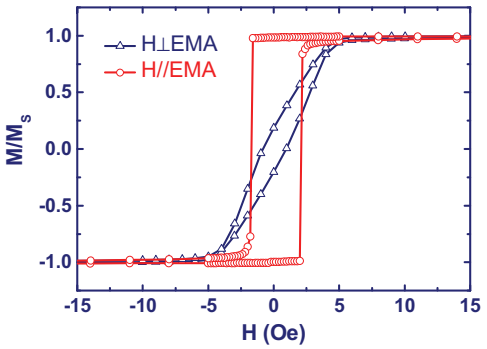

FIG. 2. (Color online) Normalized magnetization as a function of applied field for sample 1. The coercive force field of the Py layer is ~2 Oe, deduced from the M-H loop measured along the EMA.

and magnetization have the required alignment. These three thermal effects exhibit different dependences on the angle between $\Delta_x T$ and H. This provides us an opportunity to distinguish them from each other. In the following we will present the detailed processes for the determination of each thermal effect in the Pt/Py hybrid structures.

A. Coexistence of the PNE, ANE, and/or SSE

To clarify the involved thermal effects, the thermal voltage is measured while cycling the magnetic field at an angle of θ with $\nabla_x T$ (Fig. 1). We find that all the data obtained can be decomposed into the form $V_T = V_0 + V_{TH}(\theta, H)$, where V_0 is the conventional thermal voltage of the electrode-Pt contact, and V_{TH} is a polarization-dependent thermal voltage, the focus of the present work. As an example, in Fig. 3 we show the angular-dependent V_{TH} for samples 1 and 5 (recorded at the hot end), which are expected to exhibit all three thermal effects. Let us look at the data of the first sample. While cycling H along the x axis ($\theta = 0°$), the V_{TH}-H relation forms a rectangular loop with a V_{TH} jump/drop of ~0.32 μV at $\pm H_c$. A similar phenomenon was also observed by Uchida *et al.*[5] and Huang *et al.*[11] in the Pt/Py system, and ascribed to the SSE or ANE. However, if H is applied at an angle of 45°/135° with respect to the x axis, a butterfly-shaped V_{TH}-H curves appear, with two unequal minimums/maximums around $\pm H_c$ and a significant baseline offset [shown by dashed lines in Fig. 3(b)] for $|H| > 10$ Oe. This may be an indication for the simultaneous occurrence of PNE and SSE/ANE. Cycling H along the y axis, we observed a complex V_{TH}-H oscillation in the low-field regime, without baseline offsetting. This phenomenon confirms the occurrence of PNE.

Compared with those of sample 1, the V_{TH}-H curves of sample 5, which owns a y-axis EMA, show similar baseline offsets as sample 1 but different detailed features in the low-field regime. The former is understandable since the EMA is unimportant under high fields, and the latter is an indication for a different magnetic process undergoing in sample 5 under low fields. From first glance, the V_{TH}-H curves for $\theta = 0°$ are combined results of the baseline offset in Fig. 3(a) and the V_{TH} oscillation in Fig. 3(c). This can be understood noting that the magnetic moment initially forms an angle of 90° with H and, therefore, will experience a spin reorientation process

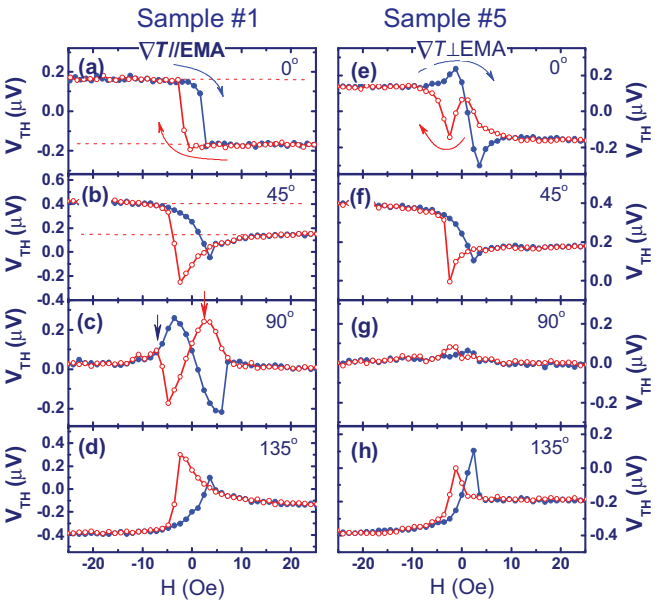

FIG. 3. (Color online) Magnetic field dependence of thermal voltage across the Pt bar at hot end; data in right and left panels correspond to samples 1 and 5, respectively. Labels in the figure mark the angle between $\nabla_x T$ and H. Red and blue curves were recorded in the field descending and ascending processes, respectively. The two arrows in (c) show two peaks of V_{TH} as field varies. Dashed lines mark the baselines of the V_{TH}-H curves.

similar to that of sample 1 for $\theta = 90°$. For the intermediate angles of $\theta = 45°$ and 135°, the V_{TH}-H curves exhibit a behavior similar to that of sample 1 except with the reversed order of the two maximums. As for sample 1, from these behaviors we find unambiguous signatures of the PNE, ANE, and/or SSE.

As well documented, heat flow carried by electrons suffers from a scattering due to spin-orbital coupling, yielding the PNE.[17] In addition to PNE, a thermal voltage V_{ANE} associated with ANE, which is also an intrinsic character of ferromagnetic materials, may occur if $\nabla_z T$ exists.[11] Both the PNE and ANE are the conventional thermoelectric effects of magnetic materials. Recently, a new effect called SSE was reported for the Pt/Py system by Uchida *et al*.[5] As proposed, spin current will be injected into Pt by temperature gradient, producing a thermal voltage described by $V_{SSE} \propto j_s \times \sigma$, where j_s is the spin current and σ the spin polarization vector. V_{PNE} is characterized by a $\sin 2\theta$ dependence,[17] whereas V_{ANE} and V_{SSE} share the same feature of $\cos\theta$ dependence.[5] It is therefore possible to identify them by quantitatively analyzing the V_{TH}-θ relation. Since it is meaningful only for fully aligned magnetic states, we performed the angular analysis only for the V_{TH} values recorded well above H_c. The V_{TH}-θ relation is obtained by averaging the V_{TH} values collected at a fixed θ but in a wide field range of 15 Oe $< |H| <$ 25 Oe. The V_{TH} values under positive and negative fields correspond to θ and $\theta + 180°$, respectively. As shown in Fig. 4, with the increase of θ, V_{TH} exhibits a complex oscillation with two unequal maximums and two unequal minimums. This result indicates the presence of more than one effect, consistent with the previous analysis on low-field data. Similar relations are obtained for samples

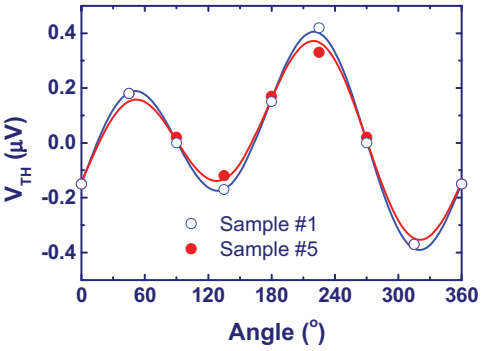

FIG. 4. (Color online) Angular dependence of thermal voltage across the Pt strip at hot end of samples 1 (empty symbols) and 5 (solid symbols). Solid lines are results calculated by $V_{TH} = k_1 \sin 2\theta - k_2 \cos\theta$.

1 and 5. It is understandable since the magnetic direction is exclusively determined by external field if $H \gg H_c$. A careful analysis reveals that the V_{TH}-θ relation can be well described by

$$V_{TH} = k_1 \sin 2\theta - k_2 \cos\theta, \quad (1)$$

adopting the parameters of $k_1 = 0.260\ \mu$V and $k_2 = 0.150\ \mu$V for sample 1 and $k_1 = 0.285\ \mu$V and $k_2 = 0.156\ \mu$V for sample 5. The satisfactory fitting of the experimental data by the $\sin 2\theta$ and $\cos\theta$ terms suggests the coexistence of the PNE and ANE/SSE. Based on the fitting parameters, the relative contributions of the PNE can be deduced, and it accounts for $k_1/(k_1 + k_2) \approx 64\%$ of the total signals. The remaining 36% may come from the ANE or SSE or both of them. V_{ANE} and V_{SSE} exhibit similar angular dependence, and their identification requires further experiments. We will return to this topic after brief discussions about the data in Fig. 3. In terms of coexisting PNE and ANE/SSE, the detailed features of the V_{TH}-H curves around $H = 0$ in Fig. 3 can be explained. Take the butterfly-shaped V_{TH}-H curve of $\theta = 45°$ [Fig. 3(b)] as an example. As H sweeps from 25 to -25 Oe, M deviates from 45° and orientates towards the x axis, leading to a gradual decrease of V_{TH}. When H sweeps through $-H_c$, the magnetic moment experiences a sudden switch to $-225°$, leaving a V_{TH} minimum at $-H_c$. A reverse M rotation occurs while H ascends from -25 to 25 Oe, and the shallowness of the V_{TH} minimum in this process is due to the ANE/SSE, which is asymmetric with respect to $\pm H$. The V_{TH}-H oscillation in Figs. 3(c) and 3(e) is a typical feature of PNE, stemming from the complex magnetic reconstruction caused by magnetic field.

B. Identification of the ANE and SSE

To finally clarify the thermal effects in V_{TH}, it is required to experimentally determine V_{ANE} and V_{SSE}. Sample 2 (Fig. 1) was fabricated for the purpose of separating the SSE. As well established, V_{SSE} stems from the spin injection from Py to Pt driven by spin pumping. For the $\nabla_x T$-induced SSE, if it exists, the spin currents from the bottom and top Py layers will have similar magnitude but opposite signs, and counteract each other. Meanwhile, $\nabla_z T$ will not produce spin injection

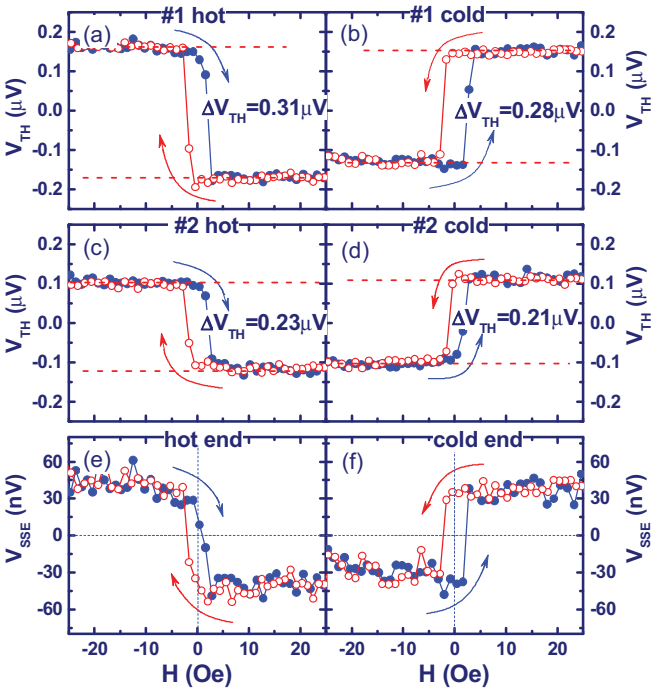

FIG. 5. (Color online) Magnetic field dependence of the thermal voltage across the Pt strip on hot and cold ends for samples 1 and 2. (a), (b) show the data for the samples with top Pt electrodes, and (c), (d) for the samples with sandwiched Pt electrodes. (e) and (f) are the pure thermal voltage associated with SSE. Red and blue curves were recorded for the field descending and ascending operations, respectively.

to the Pt strip since the latter is buried exactly in the middle of the Py layer; it is the center of the $\nabla_z T$ and where the spin distribution is symmetric. These analyses imply that in sample 2 the SSE will be completely depressed, and only the ANE survives if we apply magnetic field along EMA. Therefore, a comparison of the thermal voltages of samples 1 and 2 may allow the separation of $V_{\rm ANE}$ and $V_{\rm SSE}$.

In Figs. 5(c) and 5(d) we show the thermal voltages of sample 2, acquired at the angle of $\theta = 0°$ for sample 2 ($V_{\rm PNE}$ vanishes at this angle). Both data obtained on hot and cold ends, respectively, are presented to confirm their self-consistency. The corresponding data of sample 1 are also provided in Figs. 5(a) and 5(b) for comparison. At first glance, the $V_{\rm TH}$-H relations of sample 2 mimic exactly those of sample 1, forming two rectangular loops with opposite chirality on the two ends of the sample. However, a careful analysis indicates that the $V_{\rm TH}$ jump at H_c of sample 2 is obviously lower than that of sample 1; it is $\sim 0.23\ \mu$V/$\sim 0.21\ \mu$V on the hot/cold end for sample 2 while $\sim 0.31\ \mu$V/$\sim 0.28\ \mu$V for sample 1. According to the preceding analysis, the $V_{\rm TH}$ jump in sample 2 should be exclusively produced by ANE, while it includes the contributions of ANE and SSE in sample 1. A careful analysis of the relative directions of H, ∇T, and the thermal electric field yielded by ∇T shows that $V_{\rm ANE}$ and $V_{\rm SSE}$ have the same sign. Therefore, the extra part of $V_{\rm TH}$ in sample 1 could be ascribed to the SSE considering the absence of PNE for $\theta = 0°$, i.e., $V_{\rm SSE} = V_{\rm TH}$ (sample 1)–$V_{\rm TH}$ (sample 2) $\approx 0.08\ \mu$V (on hot end) or $\sim 0.07\ \mu$V (on cold end). In Figs. 5(e) and 5(f) we show the $V_{\rm SSE}$ as a function of magnetic field, deduced for the hot and cold ends of the sample.

C. Respective contributions of PNE, ANE, and SSE to thermal voltage

According to the previous analyses, $V_{\rm ANE}$ is $\sim 0.22\ \mu$V and $V_{\rm SSE}$ is $\sim 0.08\ \mu$V for the present experiment setup. The latter is about one third of that of the former. Noting that $V_{\rm PNE}$ takes up $\sim 64\%$ of $V_{\rm TH}$, the relative contributions of different effects can be directly calculated as follows: $V_{\rm PNE}$:$V_{\rm ANE}$:$V_{\rm SSE} \approx 0.53\ \mu$V : $0.23\ \mu$V:$0.08\ \mu$V ≈ 64:26:10. This result indicates that the dominant thermoelectric effect is PNE, and the next one is ANE. Compared with the first two effects, SSE is less important but still sizable.

However, in the above derivations the shunting effect of Pt and Py on detected thermal voltages has not been considered. It could be strong because of the high conductivity of Py and Pt. To determine the intrinsic contributions of the PNE, ANE, and SSE, a revision to the above results is necessary. Following Ramos *et al.*,[18] we have two equations for the current density along the y axis,

$$J^Y_{\rm Py} = \sigma_{\rm Py} E_Y - \alpha^{ZY}_{\rm Py} \nabla_Z T_{\rm Py} - \chi^{XY}_{\rm Py} \nabla_X T_{\rm Py},$$
$$J^Y_{\rm Pt} = \sigma_{\rm Pt} E_Y - \sigma_{\rm Pt} S^{ZY}_{\rm Py} \nabla_Z T_{\rm Py} - \sigma_{\rm Pt} S^{XY}_{\rm Py} \nabla_X T_{\rm Py},$$

where J^Y_m and σ_m are, respectively, the current density and conductivity of the m layer along the y axis (m = Py, Pt), E_Y is the thermoelectric field, $\alpha^{ZY}_{\rm Py}$ is an element of the conductivity-thermopower tensor, $\chi^{XY}_{\rm Py}$ is a parameter associated with PNE, and $S^{ZY}_{\rm Py}$ and $S^{XY}_{\rm Py}$ are the parameters associated with SSE. Setting $A_{\rm Py} J^Y_{\rm Py} + A_{\rm Pt} J^Y_{\rm Pt} = 0$, after direct derivations we obtain

$$E_Y = \frac{A_{\rm Py}\left(\alpha^{ZY}_{\rm Py} \nabla_Z T_{\rm Py} + \chi^{XY}_{\rm Py} \nabla_X T_{\rm Py}\right) + A_{\rm Pt}\left(\sigma_{\rm Pt} S^{ZY}_{\rm Py} \nabla_Z T_{\rm Py} + \sigma_{\rm Pt} S^{XY}_{\rm Py} \nabla_X T_{\rm Py}\right)}{A_{\rm Py}\sigma_{\rm Py} + A_{\rm Pt}\sigma_{\rm Pt}}$$
$$= \left(\frac{A_{\rm Py}\sigma_{\rm Py}}{A_{\rm Py}\sigma_{\rm Py} + A_{\rm Pt}\sigma_{\rm Pt}}\right) E_{\rm ANE} + \left(\frac{A_{\rm Py}\sigma_{\rm Py}}{A_{\rm Py}\sigma_{\rm Py} + A_{\rm Pt}\sigma_{\rm Pt}}\right) E_{\rm PNE} + \left(\frac{A_{\rm Pt}\sigma_{\rm Pt}}{A_{\rm Py}\sigma_{\rm Py} + A_{\rm Pt}\sigma_{\rm Pt}}\right) E_{\rm SSE}, \quad (2)$$

where

$$E_{\rm ANE} = \frac{\alpha^{ZY}_{\rm Py} \nabla_Z T_{\rm Py}}{\sigma_{\rm Py}}, \quad E_{\rm PNE} = \frac{\chi^{XY}_{\rm Py} \nabla_X T_{\rm Py}}{\sigma_{\rm Py}}, \quad E_{\rm SSE} = S^{ZY}_{\rm Py} \nabla_Z T_{\rm Py} + S^{XY}_{\rm Py} \nabla_X T_{\rm Py}. \quad (3)$$

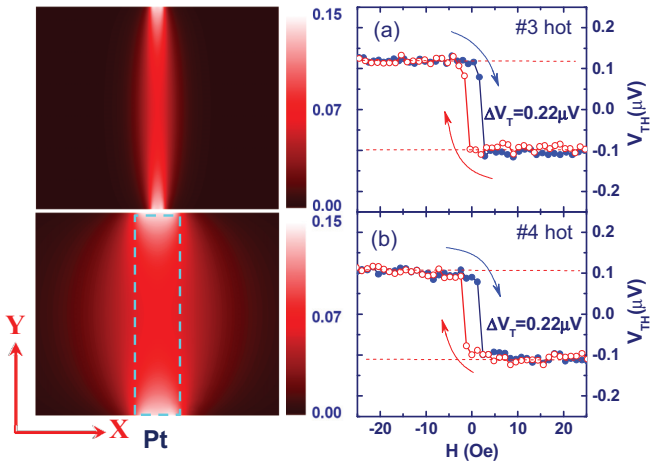

FIG. 6. (Color online) (Left panel) Distribution of E_Y in an arbitrary x-y plane in Py layer when a constant voltage (for example, 0.36 mV) across the Pt strip exists, obtained by finite element analysis. The plane dimension is 8×3 mm^2 for the Py layer and 0.1×3 mm^2 for the Pt strip. For clarity, the field mappings shown here are not presented in scale. The bottom panel is a close view of the central part of the Py layer underneath the Pt strip (marked by dashed lines). Scale bar marks the intensity of E_Y in V/m. (Right panel): Magnetic field dependence of the thermal voltage across the Pt strip for samples 3 (a) and 4 (b). Only the data collected on the hot end of the samples are presented. Red and blue curves were recorded for the field descending and ascending operations, respectively.

$A_{\rm Py}$ and $A_{\rm Pt}$ are, respectively, the areas of the Py and Pt films with normal to y direction. These results indicate that $V_{\rm SSE}$ has been reduced by a factor of $A_{\rm Pt}\sigma_{\rm Pt}/(A_{\rm Py}\sigma_{\rm Py}+A_{\rm Pt}\sigma_{\rm Pt})$ whereas $V_{\rm ANE}$ and $V_{\rm PNE}$, by a factor of $A_{\rm Py}\sigma_{\rm Py}/(A_{\rm Py}\sigma_{\rm Py}+A_{\rm Pt}\sigma_{\rm Pt})$. $A_{\rm Pt}$ is 0.1 mm $\times$ 5 nm. However, $A_{\rm Py}$ is not so easy to determine if only a part of the Py layer produces a shunting effect on Pt since the former is much wider than the latter. Considering the fact that $A_{\rm Py}$ is actually the cross section of the Py layer affected by the electric field in the Pt strip, we can calculate, via finite element analysis, the induced electric field in the Py layer when a constant voltage drop across the Pt strip exists. We found that the E_Y distribution is essentially the same in different x-y planes along the z direction but varies severely across the plane, and the E_Y is confined within a narrow strip underneath the Pt bar (top panel of Fig. 6). The y-axis currents through the Pt and Py layers can be directly calculated via

$$I_{\rm Py} = \int_{\Sigma_{\rm Py}} \sigma_{\rm Py} E_Y(x, y = 0, z)\,dx\,dz,$$

$$I_{\rm Pt} = \int_{\Sigma_{\rm Pt}} \sigma_{\rm Pt} E_Y(x, y = 0, z)\,dx\,dz,$$

and an $I_{\rm Py}$:$I_{\rm Pt}$ ratio of 9.1:1 is obtained adopting the parameters of $\Sigma_{\rm Pt} \approx 3.2 \times 10^6\ \Omega^{-1}\,{\rm m}^{-1}$ and $\sigma_{\rm Py} \approx 2.9 \times 10^6\ \Omega^{-1}\,{\rm m}^{-1}$, where $\Sigma_{\rm Py} = 8$ mm $\times$ 50 nm and $\Sigma_{\rm Pt} = 0.1$ mm $\times$ 5 nm, are the cross sections of the Py and Pt layer, respectively. Here the integration is conducted over the x-z plane of $y = 0$. The result is similar on an arbitrary x-z plane due to charge conservation. Substituting this ratio $I_{\rm Py}/I_{\rm Pt} = A_{\rm Py}\sigma_{\rm Py}/A_{\rm Pt}\sigma_{\rm Pt} \approx 9.4$ into Eqs. (2) and (3), we obtain $V_{\rm PNE}$:$V_{\rm ANE}$:$V_{\rm SSE} \approx 0.59\ \mu$V$:0.25\ \mu$V:0.83 μV $\approx$ 35:15:50. We finally come to the conclusion that the SSE in the Pt/Py hybrid structure is strong, even exceeding PNE and ANE. The Py layer is much thicker than the Pt strip; thus the SSE is strongly depressed by the shunting effect though PNE and ANE are less affected.

In fact, the ANE can be expressed as $E_{\rm ANE} = \chi S_{\rm Seeb} \nabla_Z {\rm T_{Py}}$, where $S_{\rm Seeb} = 20\ \mu$V/K (Ref. 5) is the Seebeck coefficient of Py and $\chi = 0.13$ for Py.[19] Based on this relation, the perpendicular temperature gradient in the Py layer can be obtained $\nabla_Z {\rm T_{Py}} = 32$ K/m, adopting $V_{\rm ANE} = 0.25\ \mu$V. This value is very similar to that deduced by Huang *et al.*[11] (about 25.7 K/m) for the same sample that is also thermally biased along the x axis. Compared with $\nabla_Z {\rm T_{Py}}$, $\nabla_X {\rm T_{Py}}$ is easy to be estimated, and it is $\sim 3.7 \times 10^3$ K/m according to our experiment setup. Following Ramos *et al.*,[18] we define a parameter describing SSE, $S_{Pt-Py} = E_{\rm SSE}/\nabla T$ [The ANE of the polarized Pt interface layer was not considered since it is much weaker than that of Py (Ref. 18)], where $\nabla T = \nabla_X {\rm T_{Py}} + \nabla_Z {\rm T_{Py}}$ assuming $\nabla_X {\rm T_{Py}}$ and $\nabla_Z {\rm T_{Py}}$ are equivalent for producing SSE. A direct calculation shows $S_{Pt-Py} \approx 74.3$ nV/K, which is a value similar to that detected in the Pt layer above Fe_3O_4 (74 nV/K).[18]

D. Brief discussions

In the above derivations, it has been tacitly granted that samples 1 and 2 have similar thermal distribution, and therefore the same $V_{\rm ANE}$ value. In the following we will give a simple analysis of the temperature profiles in samples 1 and 2 to assure the plausibility of this assumption. The analyses below are based on two assumptions: First, the heat absorbed from the heater is exactly the same for samples 1 and 2. Second, the absorbed heat is either dissipated in the environment via thermal convection/radiation or transferred to a cold block. In general, the heat transfer rate per unit surface can be expressed as $Q = Q_1 + Q_2 + Q_3 = h(T - T_0) + \varepsilon\sigma T^4 + \lambda\Delta T$, where h is the convective heat transfer coefficient, ϵ is the emissivity coefficient, and σ is the Stefan-Boltzmann constant, T_0 is the room temperature for the present experiments, $1/\lambda$ is the thermal resistance of the Si-Cu interface, and ΔT is the temperature difference of Si and Cu. The first two terms describe the heat released through the sample surface. In general, $h = 5$–$30\ {\rm W\,m^{-2}\,K^{-1}}$ for natural air convection, $\epsilon \approx 0.03$ (22 °C) for polished Pt, ~ 0.04 (22 °C) for Ni (22 °C), and ~ 0.14 for Fe (38 °C), $\sigma = 5.67 \times 10^{-8}\ {\rm W\,m^{-2}\,K^{-4}}$.[20] We failed to find the emissivity coefficient of Py, and will approximate it by an average of those of Ni and Fe ($0.8\epsilon_{\rm Ni} + 0.2\epsilon_{\rm Fe} = 0.06$). The emissivity coefficient of Pt is lower than that of Py, and this results in a reduction of $\sim 0.055\kappa(Q_1 + Q_2)$ in the heat dissipated through sample surface, adopting the parameters of $h = 10\ {\rm W\,m^{-2}\,K^{-1}}$ (an intermediate value for natural air convection), $T = (273.16 + 50)$ K and $T_0 = (273.16 + 20)$ K, where κ is the ratio of the surface area of the Pt bar to that of the entire sample.

Let us consider two limit cases. Firstly, the surface temperature of Pt in sample 1 increases to completely dissipate the additional $0.055\kappa(Q_1 + Q_2)$. In this case, the temperature profile in sample 1 will be exactly the same as that of sample 2. Another limit is that the residual $0.055\kappa(Q_1 + Q_2)$ is

transferred either by the remaining sample surface apart from Pt or by cold block. In this case the $\nabla_Z T_{\mathrm{Py}}$ in the Py layer underneath the Pt strip will be decreased by $-0.055\nabla_Z T_{\mathrm{Py}}$. In an actual situation, the temperature gradient may take a value between $\sim 0.945\nabla_Z T_{\mathrm{Py}}$ and $\nabla_Z T_{\mathrm{Py}}$. These analyses indicate that, at least, the V_{ANE} of sample 1 will not exceed that of sample 2; i.e., the enhanced V_{TH} in sample 1 should have a distinct origin.

The following investigations on samples 3 and 4 (right panel of Fig. 6) provide lateral evidence for the invariance of temperature distribution while shifting sandwiched Pt to Py surface. As shown by Figs. 6(a) and 6(b), samples 3 and 4 exhibit essentially the same V_{TH}-H loop with a V_{TH} jump of ~ 0.22 μV, at the hot side, or ~ 0.20 μV, at the cold side (not shown). This phenomenon has only one explanation, i.e., the SSE is absent not only in sample 4 but also in sample 3, and the detected V_{TH} change is simply V_{ANE}. Remarkably, the V_{ANE} values obtained here are in good agreement with those of samples 1 and 2. The invariance of V_{ANE} indicates that, as expected, the thermal distribution in the samples are unaffected by the location/thickness change of the Pt strips.

The observation for the disappearance of the SSE in the Pt layers of 2 nm is interesting. This phenomenon may be explained in terms of spin current cancellation. As well established, the SSE stems from an electric field-induced asymmetric deflection of the electrons with opposite spin orientations. For a sample with a thickness well below spin diffusion, the spin current coming from one Py-Pt interface has the probability to reach the opposite interface and then be reflected back into the Pt layer. The reflected spin current has the opposite direction but similar spin polarization as the original one, counteracting most of the effects of the latter.[21] As reported, the spin diffusion length of Pt is ~ 5 nm,[22] well above the thickness of the Pt layers in samples 3 and 4.

IV. CONCLUSIONS

We presented a systematic study on thermoelectric effect for the Pt/Py systems by deliberately designing sample structure to identify the contributions of different thermal effects. Characteristics of spin Seebeck effect (SSE), anomalous Nernst effect (ANE), and planar Nernst effect (PNE) are recognized from the field-dependent thermal voltages across the Pt strips when a thermal gradient exists. By comparing the data of differently structured samples, the respective contributions of the PNE, ANE, and SSE to thermal voltage are determined, and they have the ratio of 64:26:10, without considering the shunting effect of conductive Py, or 35:15:50, after the shunting-effect correction.

ACKNOWLEDGMENTS

This work has been supported by the National Basic Research Program of China, the National Natural Science Foundation of China, the Knowledge Innovation Project of the Chinese Academy of Science, and the Beijing Municipal Nature Science Foundation.

*Author to whom correspondence should be addressed: jrsun@iphy.ac.cn

[1] S. A. Crooker, M. Furis, X. Lou, C. Adelmann, D. L. Smith, C. J. Palmstrøm, and P. A. Crowell, Science **309**, 2191 (2005).
[2] Y. K. Kato, R. C. Myers, A. C. Gossard, and D. D. Awschalom, Science **306**, 1910 (2004).
[3] J. Wunderlich, B. Kaestner, J. Sinova, and T. Jungwirth, Phys. Rev. Lett. **94**, 047204 (2005).
[4] Y. Tserkovnyak, A. Brataas, and G. E. W. Bauer, Phys. Rev. Lett. **88**, 117601 (2002).
[5] K. Uchida, S. Takahashi, K. Harii, J. Ieda, W. Koshibae, K. Ando, S. Maekawa, and E. Saitoh, Nature **455**, 778 (2008).
[6] S. Bosu, Y. Sakuraba, K. Uchida, K. Saito, T. Ota, E. Saitoh, and K. Takanashi, Phys. Rev. B **83**, 224401 (2011).
[7] C. M. Jaworski, J. Yang, S. Mack, D. D. Awschalom, J. P. Heremans, and R. C. Myers, Nat. Mater. **9**, 898 (2010).
[8] K. Uchida, J. Xiao, H. Adachi, J. Ohe, S. Takahashi, J. Ieda, T. Ota, Y. Kajiwara, H. Umezawa, H. Kawai, G. E. W. Bauer, S. Maekawa, and E. Saitoh, Nat. Mater. **9**, 894 (2010).
[9] K. Uchida, H. Adachi, T. Ota, H. Nakayama, S. Maekawa, and E. Saitoh, Appl. Phys. Lett. **97**, 172505 (2010).
[10] C. M. Jaworski, R. C. Myers, E. Johnston-Halperin, and J. P. Heremans, Nature **487**, 210 (2012).
[11] S. Y. Huang, W. G. Wang, S. F. Lee, J. Kwo, and C. L. Chien, Phys. Rev. Lett. **107**, 216604 (2011).
[12] S. Y. Huang, X. Fan, D. Qu, Y. P. Chen, W. G. Wang, J. Wu, T. Y. Chen, J. Q. Xiao, and C. L. Chien, Phys. Rev. Lett. **109**, 107204 (2012).
[13] D. Qu, S. Y. Huang, J. Hu, R. Wu, and C. L. Chien, Phys. Rev. Lett. **110**, 067206 (2013).
[14] A. D. Avery, M. R. Pufall, and B. L. Zink, Phys. Rev. Lett. **109**, 196602 (2012).
[15] T. Kikkawa, K. Uchida, Y. Shiomi, Z. Qiu, D. Hou, D. Tian, H. Nakayama, X. F. Jin, and E. Saitoh, Phys. Rev. Lett. **110**, 067207 (2013).
[16] D. Meier, T. Kuschel, L. Shen, A. Gupta, T. Kikkawa, K. Uchida, E. Saitoh, J. M. Schmalhorst, and G. Reiss, Phys. Rev. B **87**, 054421 (2013).
[17] V. D. Ky, Phys. Status Solidi **17**, K207 (1966).
[18] R. Ramos, T. Kikkawa, K. Uchida, H. Adachi, I. Lucas, M. H. Aguirre, P. Algarabel, L. Morellon, S. Maekawa, E. Saitoh, and M. R. Ibarra, Appl. Phys. Lett. **102**, 072413 (2013).
[19] A. Slachter, F. L. Bakker, and B. J. van Wees, Phys. Rev. B **84**, 020412(R) (2011).
[20] W. L. Wolfe and G. J. Zissis, *The Infrared Handbook* (Office of Naval Research, Department of the Navy, Washington, DC, 1985); W. L. Wolfe, *Handbook of Military Infrared Technology* (Office of Naval Research, Department of the Navy, Washington, DC, 1965).
[21] H. Nakayama, M. Althammer, Y.-T. Chen, K. Uchida, Y. Kajiwara, D. Kikuchi, T. Ohtani, S. Geprägs, M. Opel, S. Takahashi, R. Gross, G. E. W. Bauer, S. T. B. Goennenwein, and E. Saitoh, Phys. Rev. Lett. **110**, 206601 (2013).
[22] J. Bass and W. P. Pratt, J. Phys-Condens. Mat. **19**, 183201 (2007).